

1 New Non-BCS Superconductivity Pairing via Chiral Electron-Hole 2 Condensation

3 Wanpeng Tan*

4 *Department of Physics and Astronomy,*
5 *University of Notre Dame, Notre Dame, Indiana 46556, USA*

6 (Dated: November 8, 2023)

A novel chiral electron-hole (CEH) pairing mechanism is proposed to account for non-BCS superconductivity. In contrast to BCS Cooper pairs, CEH pairs exhibit a pronounced affinity to antiferromagnetism for superconductivity. The gap equations derived from this new microscopic mechanism are analyzed for both s- and d-wave superconductivity, revealing marked departures from the BCS theory. Unsurprisingly, CEH naturally describes superconductivity in strongly-correlated systems, necessitating an exceedingly large coupling parameter ($\lambda > 1$ for s-wave and $\lambda > \pi/2$ for d-wave) to be efficacious. The new mechanism provides a better understanding of various non-BCS features, especially in cuprate and iron-based superconductors. In particular, CEH, through quantitative comparison with experimental data, shows promise in solving long-standing puzzles such as the unexpectedly large gap-to-critical-temperature ratio Δ_0/T_c , the lack of gap closure at T_c , superconducting phase diagrams, and a non-zero heat-capacity-to-temperature ratio C/T at $T = 0$ (i.e., the “anomalous linear term”), along with its quadratic behavior near $T = 0$ for d-wave cuprates.

7 I. INTRODUCTION

8 Magnetism has traditionally been viewed as antagonistic to conventional Bardeen-
9 Cooper-Schrieffer (BCS) superconductivity [1]. However, many non-BCS superconductors
10 discovered in the past few decades have demonstrated the opposite, showing that strong
11 magnetism is actually very conducive to non-BCS superconductivity. In particular, many of
12 them are derived from parent compounds with antiferromagnetic properties, and some even
13 exhibit cases of the coexistence of superconductivity and antiferromagnetic order [2]. The
14 two primary classes of high T_c superconductors, cuprate [3] and iron-based (FeSC) [4] super-
15 conductors, both have their roots in antiferromagnetic compounds, with cuprates originating
16 from antiferromagnetic Mott insulators and FeSCs from antiferromagnetic metals.

17 The coexistence of superconductivity and long-range antiferromagnetic order was actually
18 discovered a long time ago in the late 1970s [5, 6]. The intimate relationship between
19 antiferromagnetism and superconductivity has been observed in many different types of
20 non-BCS superconducting materials, including heavy fermion compounds [7, 8], organic
21 superconductors such as quasi-1D TMTTF/TMTSF type and quasi-2D BEDT-TTF type
22 [9], and doped fullerenes [10].

23 The significance of antiferromagnetic order may provide crucial clues for solving the
24 puzzles of non-BCS superconductivity. In particular, this leads to our proposal of a new

* wtan@nd.edu

25 pairing mechanism via chiral electron-hole (CEH) condensation in this work. The presence
 26 of strong antiferromagnetic correlations is critical, as it guarantees that chirally opposite
 27 electron and hole states are next to each other, making the chiral condensation more feasible.
 28 This may explain why both high T_c superconducting classes (cuprates and FeSCs) are based
 29 on antiferromagnetic compounds.

30 In order to fully comprehend these superconductors, it is imperative to not only find
 31 their correct pairing mechanism, but also to identify their pairing symmetry. Angle-resolved
 32 photoemission spectroscopy measurements have indisputably proven that cuprates display
 33 a $d_{x^2-y^2}$ gap symmetry [11]. Although studies on the pairing symmetry of FeSCs that were
 34 discovered much later are not as conclusive, the majority consensus suggests that they most
 35 probably exhibit some type of s-wave pairing symmetry [12].

36 In this paper, we apply the mean-field approach to derive superconducting gap equations
 37 using the new pairing mechanism. Detailed analysis of the equations for both s-wave and
 38 d-wave superconductivity will reveal various features that differ from BCS. Furthermore, we
 39 will address puzzles concerning superconducting gap and heat capacity and present several
 40 examples that directly compare CEH predictions with cuprate and FeSC data. Natural units
 41 ($\hbar = c = k_B = 1$) are utilized throughout the work for convenience.

42 II. CHIRAL ELECTRON-HOLE (CEH) PAIRING

43 We will closely follow the Bogoliubov-BCS formalism as described in Ref. [13] for the
 44 mean-field theory of BCS superconductivity, albeit with a new microscopic superconducting
 45 mechanism. First of all, we will begin with a four-fermion interacting Hamiltonian for the
 46 simple straightforward case of s-wave CEH pairing,

$$H = \sum_{\mathbf{k}\sigma} \xi_{\mathbf{k}} c_{\mathbf{k}\sigma}^\dagger c_{\mathbf{k}\sigma} - V \sum_{\mathbf{k}\mathbf{k}'} c_{\mathbf{k}L}^\dagger c_{-\mathbf{k}R} c_{-\mathbf{k}'R}^\dagger c_{\mathbf{k}'L} \quad (1)$$

47 where we use left and right chiralities instead of the conventional up and down spin notation
 48 to emphasize the significance of chirality in this study.

49 Note that similar four-fermion interactions were also used in the Nambu-Jona-Lasinio
 50 (NJL) mechanism [14] in particle physics for quark condensation and spontaneous symmetry
 51 breaking, borrowing the idea from the earlier BCS superconductivity work [1]. Such ideas
 52 are also crucial in the recently developed mirror matter theory, which aims to address many
 53 puzzles in fundamental physics and cosmology [15–19]. In particular, the concept of staged
 54 chiral quark condensation [16, 19, 20] has directly motivated this work.

55 The most significant difference in Eq. 1 from the BCS Hamiltonian is that, by borrowing
 56 back the idea of the NJL model, the four creation and annihilation operators are arranged
 57 to incorporate the proposed condensation mechanism of chiral electron-hole pairs instead
 58 of the conventional Cooper pairs. Specifically, the superconducting pairs are formed from
 59 electrons and holes with exactly opposite chiralities, a configuration readily achievable in
 60 adjacent sites of antiferromagnetic materials. We can then define a similar order parameter
 61 Δ based on the CEH condensation mechanism,

$$\Delta = V \sum_{\mathbf{k}} \langle c_{\mathbf{k}L}^\dagger c_{-\mathbf{k}R} \rangle, \quad \Delta^* = V \sum_{\mathbf{k}} \langle c_{-\mathbf{k}R}^\dagger c_{\mathbf{k}L} \rangle. \quad (2)$$

62 Upon initial instinctive consideration, one might assume that CEH pairs cannot conduct
 63 electric currents due to their zero net charge. However, the conduction mechanism of CEH

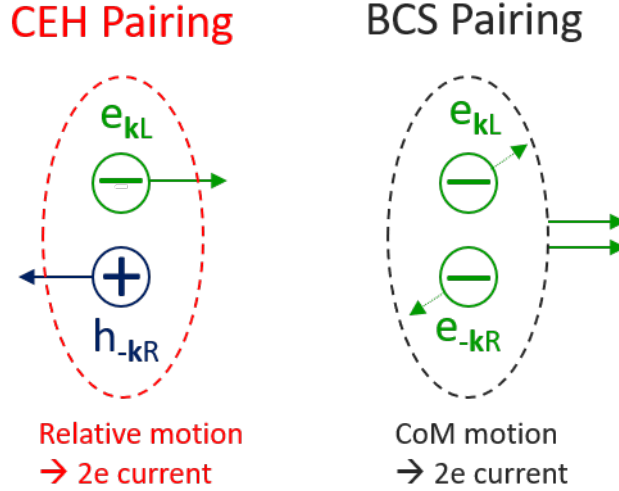


FIG. 1. Different pairing and conducting mechanisms between CEH and BCS are shown.

64 pairs is fundamentally different from that of Cooper pairs, as illustrated in Fig. 1. While the
 65 Cooper pair conducts currents through center-of-mass motion, the CEH pair achieves this
 66 through relative motion. On a macroscopic scale, both mechanisms yield equivalent $2e$ -like
 67 currents, resulting in comparable outcomes in most macroscopic phenomena, including the
 68 Josephson effect.

69 Another important aspect concerns the pairing symmetry. In CEH condensation, the
 70 pairs must be spin singlets owing to its chiral nature (like the Higgs in particle physics),
 71 leading to symmetric orbital wave functions. Consequently, the resulting pairing symmetry
 72 can only be s -, d -, or g -wave.

73 Considering the CEH condensation, the Hamiltonian of Eq. 1 then takes the bilinear
 74 form,

$$H = \sum_{\mathbf{k}} (c_{\mathbf{k}L}^\dagger, c_{-\mathbf{k}R}^\dagger) \begin{pmatrix} \xi_{\mathbf{k}} & -\Delta^* \\ -\Delta & \xi_{\mathbf{k}} \end{pmatrix} \begin{pmatrix} c_{\mathbf{k}L} \\ c_{-\mathbf{k}R} \end{pmatrix}. \quad (3)$$

75 We can then diagonalize the Hamiltonian through the Bogoliubov transformation [21] as
 76 follows,

$$U^\dagger \begin{pmatrix} \xi_{\mathbf{k}} & -\Delta^* \\ -\Delta & \xi_{\mathbf{k}} \end{pmatrix} U = \begin{pmatrix} E_{\mathbf{k}}^+ & 0 \\ 0 & E_{\mathbf{k}}^- \end{pmatrix}, \quad U = \begin{pmatrix} u_{\mathbf{k}} & v_{\mathbf{k}}^* \\ -v_{\mathbf{k}} & u_{\mathbf{k}}^* \end{pmatrix} \quad (4)$$

77 where the eigenvalues are,

$$E_{\mathbf{k}}^\pm = \xi_{\mathbf{k}} \pm |\Delta|, \quad (5)$$

78 in contrast to $E_{\mathbf{k}}^\pm = \pm \sqrt{\xi_{\mathbf{k}}^2 + |\Delta|^2}$ in BCS. The corresponding emergent Bogoliubov quasi-
 79 particles are therefore defined as follows,

$$\begin{pmatrix} b_{\mathbf{k}L} \\ b_{-\mathbf{k}R} \end{pmatrix} = U^\dagger \begin{pmatrix} c_{\mathbf{k}L} \\ c_{-\mathbf{k}R} \end{pmatrix} \quad (6)$$

80 where the quasi-particle operators b and b^\dagger satisfy the same anticommutation relations as
 81 fermions. Applying the unitarity condition of $|u|^2 + |v|^2 = 1$, we arrive at the solution,

$$|u| = |v| = \frac{1}{\sqrt{2}} \quad (7)$$

82 which is remarkably different from the BCS findings. To facilitate later discussion, we can
83 introduce a phase factor by setting $u/v = e^{i\delta}$, which gives $u^*v = 1/2e^{-i\delta}$.

84 Using the above solution, we obtain the following condensation relation

$$\langle c_{\mathbf{k}L}^\dagger c_{-\mathbf{k}R} \rangle = u^*v (\langle b_{-\mathbf{k}R}^\dagger b_{-\mathbf{k}R} \rangle - \langle b_{\mathbf{k}L}^\dagger b_{\mathbf{k}L} \rangle) \quad (8)$$

85 where, at finite temperature, the quasi-particles follow Fermi-Dirac statistics, that is,

$$\langle b_{\mathbf{k}L}^\dagger b_{\mathbf{k}L} \rangle = \frac{1}{e^{E^+/T} + 1}, \quad \langle b_{-\mathbf{k}R}^\dagger b_{-\mathbf{k}R} \rangle = \frac{1}{e^{E^-/T} + 1}. \quad (9)$$

86 Then, we can obtain the s-wave CEH gap equation from Eqs. 2, 5, 8, and 9,

$$\begin{aligned} \Delta &= \frac{V}{2} e^{-i\delta} \sum_{\mathbf{k}} \frac{\sinh(|\Delta|/T)}{\cosh(|\Delta|/T) + \cosh(\xi_{\mathbf{k}}/T)} \\ &= V \rho_F e^{-i\delta} \int_0^{\omega^*} d\xi \frac{\sinh(|\Delta|/T)}{\cosh(|\Delta|/T) + \cosh(\xi/T)} \end{aligned} \quad (10)$$

87 where ρ_F denotes the density of states at the Fermi energy and the summation is replaced
88 by an integration over the energy shell ($\pm\omega^*$) near the Fermi surface where the formation
89 of superconducting pairs occurs. It is worth noting that ω^* bears resemblance to the Debye
90 energy ω_D in the BCS theory. However, we will elaborate later on the more significant
91 impact of ω^* within the CEH mechanism.

92 By working out the integration and introducing a dimensionless coupling parameter $\lambda =$
93 $V \rho_F$ and a positive energy gap Δ defined by $\Delta = \Delta e^{-i\delta}$, the s-wave gap equation can be
94 simplified as,

$$\begin{aligned} \Delta(T) &= 2\lambda T \tanh^{-1} \left(\tanh\left(\frac{\Delta(T)}{2T}\right) \tanh\left(\frac{\omega^*}{2T}\right) \right) \\ &= \lambda T \log\left(\frac{e^{(\Delta(T)+\omega^*)/T} + 1}{e^{\Delta(T)/T} + e^{\omega^*/T}}\right). \end{aligned} \quad (11)$$

95 CEH Gap equations with more intricate orbital pairing symmetries can be calculated by
96 considering an angular-dependent superconducting energy gap $\Delta_{\mathbf{k}} = \Delta \gamma_{\mathbf{k}}$. For a d-wave gap
97 symmetry of $d_{x^2-y^2}$ in cuprate superconductors, we have the symmetry factor $\gamma_{\mathbf{k}} = \cos(2\varphi)$.
98 A d-wave CEH gap equation can then be derived with ease,

$$\Delta(T) = \frac{8\lambda T}{\pi} \int_0^{\pi/4} d\varphi \tanh^{-1} \left(\tanh\left(\frac{\Delta(T) \cos(2\varphi)}{2T}\right) \tanh\left(\frac{\omega^*}{2T}\right) \right). \quad (12)$$

99 If we further consider Δ as an emergent scalar field (akin to the Higgs field in parti-
100 cle physics), its self-interactions will lead to the same phenomenological Ginsburg-Landau
101 theory as derived in BCS superconductivity.

102 III. ANALYSIS OF CEH GAP EQUATIONS

103 First, we should emphasize that both s-wave and d-wave gap equations in CEH (Eqs. 11
104 and 12) are dramatically different from those derived in the BCS theory. In particular, the

105 two parameters of ω^* and λ play a crucial role in distinguishing the CEH mechanism from
106 BCS.

107 To ensure that quasi-particles have positive energies (or negative energies for correspond-
108 ing “anti-particles”) as in Eq. 5, we establish the following superconducting requirement
109 under the CEH model,

$$\omega^* \leq \Delta(T) \quad (13)$$

110 which is entirely different from that of BCS. In BCS, positive energies are guaranteed as
111 $E_{\mathbf{k}}^+ = \sqrt{\xi_{\mathbf{k}}^2 + |\Delta|^2}$, and thus no constraint on the Debye energy ω_D is necessary. In addition,
112 it should be noted that the coupling parameter λ in CEH must be very large (i.e., $\lambda > 1$ for
113 s-wave and $\lambda > \pi/2$ for d-wave as presented below), as opposed to the small parameter of
114 $\lambda \ll 1$ used in BCS. This implies that CEH is naturally suited for modeling superconductivity
115 in strongly-correlated electron systems while BCS is more appropriate for the weak-coupling
116 limit.

117 The condition of Eq. 13 suggests that typically $\Delta(T_c) = \omega^* \neq 0$, meaning that the
118 superconducting gap does not necessarily close at the critical temperature T_c , which is
119 distinct from BCS. More details are presented below for both s- and d-wave cases.

120 A. s-wave results

121 The CEH s-wave gap equation (Eq. 11) can also be written as,

$$x^{1/\lambda}(x + w) = wx + 1 \quad (14)$$

122 where $x = \exp(\Delta(T)/T) > 1$ and $w = \exp(\omega^*/T) > 1$. The superconducting condition of
123 Eq. 13 requires that $x > w$. We can then easily solve it for λ ,

$$\lambda = \frac{\log(x)}{\log\left(\frac{wx+1}{w+x}\right)} = \frac{\log(x)}{\log(x) + \log\left(\frac{w+1/x}{w+x}\right)} > 1 \quad (15)$$

124 which means that CEH addresses a strongly-correlated system.

125 In the limit of $T \rightarrow 0$, we obtain the gap at zero temperature,

$$\Delta_0 \equiv \Delta(T = 0) = \lambda\omega^* \quad (16)$$

126 and the gap equation can then be simplified at the critical temperature T_c as,

$$2 \exp\left(\frac{\lambda + 1}{\lambda^2} \frac{\Delta_0}{T_c}\right) = \exp\left(\frac{2}{\lambda} \frac{\Delta_0}{T_c}\right) + 1. \quad (17)$$

127 This allows us to plot the solution of Δ_0/T_c as a function of λ as shown in Fig. 2 with its
128 two asymptotic limits: two as $\lambda \rightarrow \infty$ and $\log(2)\lambda^2/(\lambda - 1)$ as $\lambda \rightarrow 1$. Note that this ratio
129 is always larger than two and can become much larger at smaller λ (or lower doping levels),
130 in contrast to the constant value of about 1.764 in BCS for s-wave superconductors.

131 Fig. 3 shows the $\Delta(T)/\Delta_0$ ratios as a function of T/T_c for various λ values, which are
132 numerically calculated from the gap equation. In Fig. 3, it is evident that the supercon-
133 ducting gap in CEH, in general, does not close at the critical temperature T_c , resulting in

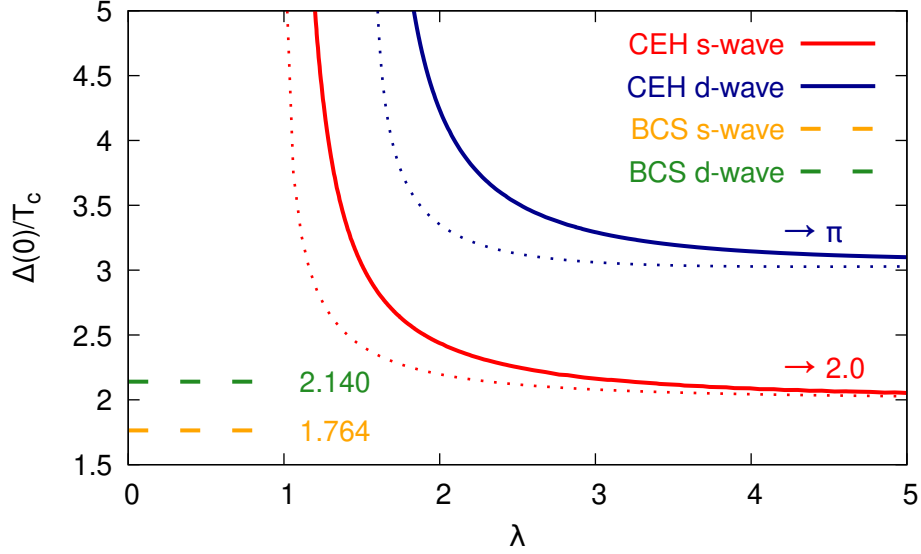


FIG. 2. Δ_0/T_c as a function of λ is shown for both s-wave and d-wave CEH superconductivity. Constant BCS values are also displayed for comparison. The two dotted lines depict Δ_0/T_0 corresponding to their respective CEH results.

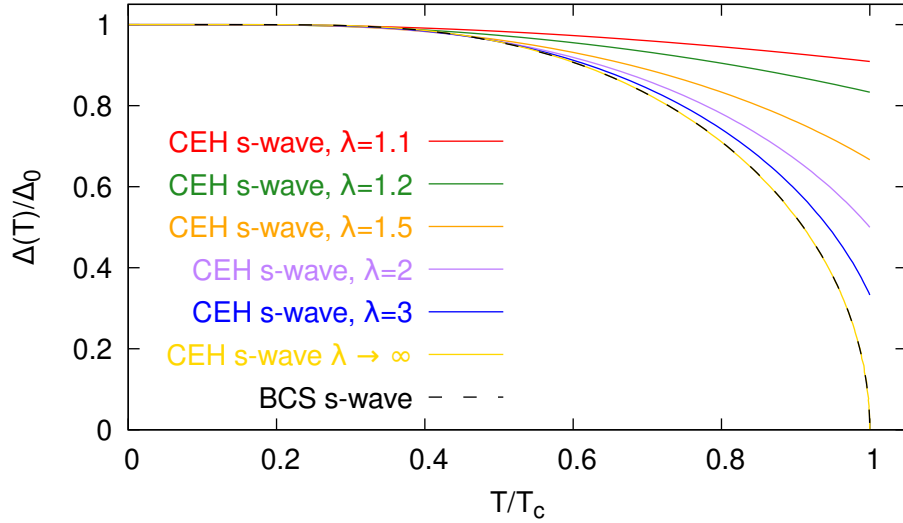


FIG. 3. The $\Delta(T)/\Delta_0$ ratios as a function of T/T_c are shown for s-wave CEH superconductivity. The gap only vanishes at T_c when $\lambda \rightarrow \infty$, in which case the curve nearly overlaps with that of BCS.

¹³⁴ $\Delta(T_c) = \Delta_0/\lambda$ according to Eq. 16. It only closes in the extreme case of $\lambda \rightarrow \infty$, where the
¹³⁵ relation between $\Delta(T)/\Delta_0$ and T/T_c can be simplified as,

$$\frac{T}{T_c} = \frac{\Delta(T)/\Delta_0}{\tanh^{-1}(\Delta(T)/\Delta_0)} \quad (18)$$

¹³⁶ which nearly overlaps with the results from BCS as shown in Fig. 3.

137 On the other hand, the superconducting gap does close at a higher temperature $T_0 > T_c$.
 138 It can be calculated from the gap equation using the condition of $\Delta(T_0) = 0$,

$$T_0 = \frac{\omega^*}{2 \tanh^{-1}(1/\lambda)} = \frac{\omega^*}{\log(\frac{\lambda+1}{\lambda-1})} \quad (19)$$

139 which, though higher, follows a similar trend as T_c as demonstrated in the following section.
 140 Another ratio can be calculated simply as follows,

$$\Delta_0/T_0 = 2\lambda \tanh^{-1}(1/\lambda) < \Delta_0/T_c \quad (20)$$

141 which is shown as the red dotted line in Fig. 2.

142 At $T \rightarrow 0$, we find, directly from the gap equation, that the energy gap exponentially
 143 approaches its maximum value of Δ_0 ,

$$\Delta(T) \simeq \Delta_0 - \lambda T \exp(-\frac{\Delta_0}{T}(1 - \frac{1}{\lambda})) \quad (21)$$

144 which is similar to that of BCS.

145

B. d-wave results

146 Taking the limit of $T \rightarrow 0$, we obtain the coupling parameter from the gap equation (Eq.
 147 12) (see Appendix A),

$$\lambda = \frac{\pi}{2(1 - \sin 2\theta) + 4\theta \cos 2\theta} > \frac{\pi}{2} \quad (22)$$

148 where θ is defined by $\cos 2\theta = \omega^*/\Delta_0$ within the range of $0 < \theta < \pi/4$. This indicates that
 149 CEH d-wave superconductors require even stronger correlations.

150 We can also obtain the d-wave ratio of Δ_0/T_c numerically from the gap equation using
 151 $\omega^* = \Delta(T_c) = \Delta_0 \cos 2\theta$ and compare it with the s-wave and BCS results, as shown in Fig.
 152 2 and also in Fig. 4 as a function of θ . The general trend of the d-wave ratio is similar to
 153 the s-wave one, though notably higher. However, the inset plot in Fig. 4 reveals that the
 154 d-wave ratio is not monotonic and has a minimum of about 3.0774 at $\theta \approx 0.7184$.

155 Similar to the s-wave results, the normalized d-wave superconducting gap as a function
 156 of T/T_c is shown in Fig. 5. Again, it does not close at T_c which is contrary to the BCS
 157 prediction. Note that the temperature dependence of the BCS d-wave gap, unlike the s-wave
 158 case, differs greatly from the CEH predictions, even in the limit of $\lambda \rightarrow \infty$ or $\theta = \pi/4$. As
 159 a matter of fact, the distinction is so significant between BCS and CEH that measurements
 160 with decent experimental precision should be pursued.

161 It is straightforward to calculate the temperature $T_0 > T_c$ where the d-wave supercon-
 162 ducting gap vanishes,

$$T_0 = \frac{\omega^*}{2 \tanh^{-1}(\pi/(2\lambda))} \quad (23)$$

163 which is similar to the s-wave result except for a larger lower bound on the coupling param-
 164 eter ($\lambda > \pi/2$). A similar ratio can also be obtained,

$$\Delta_0/T_0 = 2 \tanh^{-1}(1 + 2\theta \cos 2\theta - \sin 2\theta) / \cos 2\theta < \Delta_0/T_c \quad (24)$$

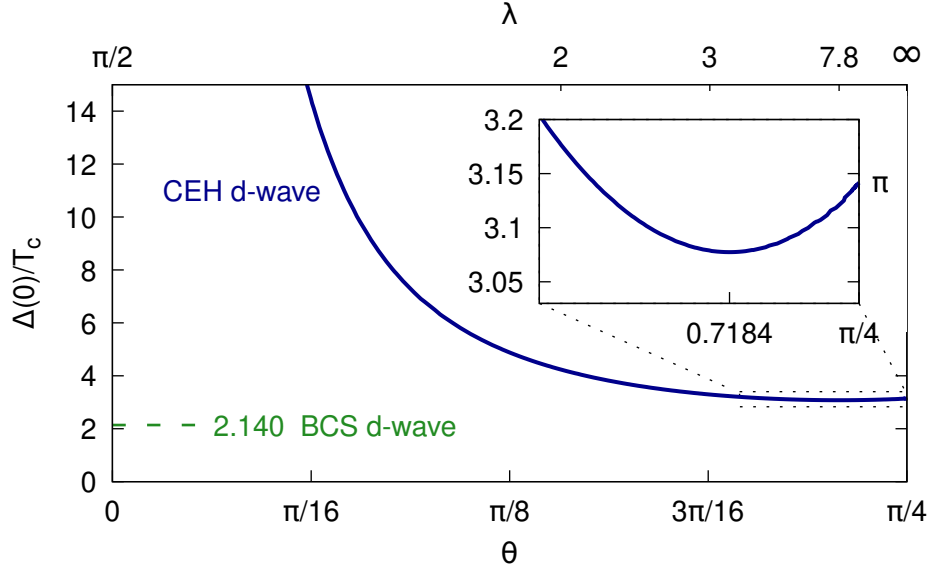


FIG. 4. The Δ_0/T_c ratios as a function of θ or λ are shown for d-wave CEH superconductivity. The inset presents a minimum of ≈ 3.0774 at $\theta \approx 0.7184$. The constant BCS d-wave value is also displayed for comparison.

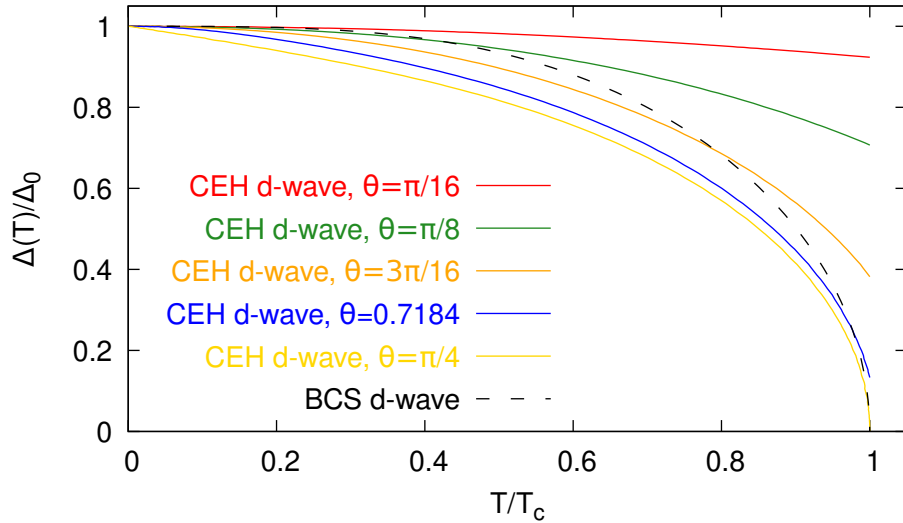


FIG. 5. The ratios of $\Delta(T)/\Delta_0$ as a function of T/T_c are shown for d-wave CEH superconductivity. The gap only closes at T_c when $\theta \rightarrow \pi/4$ or $\lambda \rightarrow \infty$. However, the gap-vanishing BCS curve behaves differently.

165 which is plotted as the blue dotted line in Fig. 2. Like Δ_0/T_c , this ratio has a minimum of
 166 about 3.027 at $\theta \approx 0.662$.

167 The asymptotic behavior of the superconducting gap at $T \rightarrow 0$ can be obtained as follows,

$$\Delta \simeq \Delta_0 - \frac{T^2}{\theta \sin(2\theta) \cos(2\theta) \Delta_0} \quad (25)$$

168 which is derived by utilizing the following integration,

$$\int_0^{\pi/4} d\varphi \exp\left(-\frac{\Delta}{T} |\cos(2\varphi) - \cos(2\theta)|\right) \Big|_{T \rightarrow 0} = \frac{T}{\Delta \sin(2\theta)}. \quad (26)$$

169

IV. ENTROPY AND SPECIFIC HEAT

170 In the CEH superconducting phase, the entropy of the finite-temperature system can be
171 expressed through the statistics of Bogoliubov quasi-particles,

$$\begin{aligned} S &= -2 \sum_{\mathbf{k}} (f_+ \log f_+ + f_- \log f_-) \\ &= -2 \sum_{\mathbf{k}} (f_+ \log f_+ + (1 - f_+) \log(1 - f_+)) \end{aligned} \quad (27)$$

172 where f_{\pm} represent the Fermi-Dirac distributions of the quasi-particles as in Eq. 9. By
173 replacing the summation with an energy integration, we obtain for the simple s-wave case,

$$S = 2 \int_{\Delta-\omega^*}^{\Delta+\omega^*} d\epsilon \rho(\epsilon) \left(\frac{\epsilon/T}{1 + e^{\epsilon/T}} + \log(1 + e^{-\epsilon/T}) \right) \quad (28)$$

174 where $\rho(\epsilon)$ is the quasi-particle density of states. This entropy formula seems to be the
175 same as the BCS one but only formally. The critical differences lie in $\rho(\epsilon)$ and the bounds
176 of integration $\pm\omega^*$. In CEH, $\rho(\epsilon) = \rho_F$, whereas in BCS, the density exhibits a singular
177 behavior at the gap energy, reflecting their differences in the pairing mechanism. More
178 significantly, the integration bounds in CEH demand more careful handling, unlike BCS, due
179 to a drastically different dispersion relation in Eq. 5. Such differences are most effectively
180 showcased in the following calculations of heat capacity.

181

A. s-wave specific heat

182 The specific heat for the CEH s-wave superconductors can be obtained from the entropy
183 in Eq. 28 as follows,

$$C_{sc} = T \frac{\partial S}{\partial T} = 2T \rho_F \int_{\Delta-\omega^*}^{\Delta+\omega^*} d\epsilon \frac{e^{\epsilon/T}}{(e^{\epsilon/T} + 1)^2} \left(\left(\frac{\epsilon}{T} \right)^2 - \frac{\epsilon}{T} \frac{\partial \Delta(T)}{\partial T} \right) \quad (29)$$

184 which can be simplified as,

$$C_{sc}(T) = 2T \rho_F (s_2(T) - \frac{\partial \Delta(T)}{\partial T} s_1(T)) \quad (30)$$

185 where the two auxiliary functions are defined as

$$s_{1,2}(T) = \int_{(\Delta-\omega^*)/T}^{(\Delta+\omega^*)/T} dx \frac{e^x}{(e^x + 1)^2} x^{1,2}. \quad (31)$$

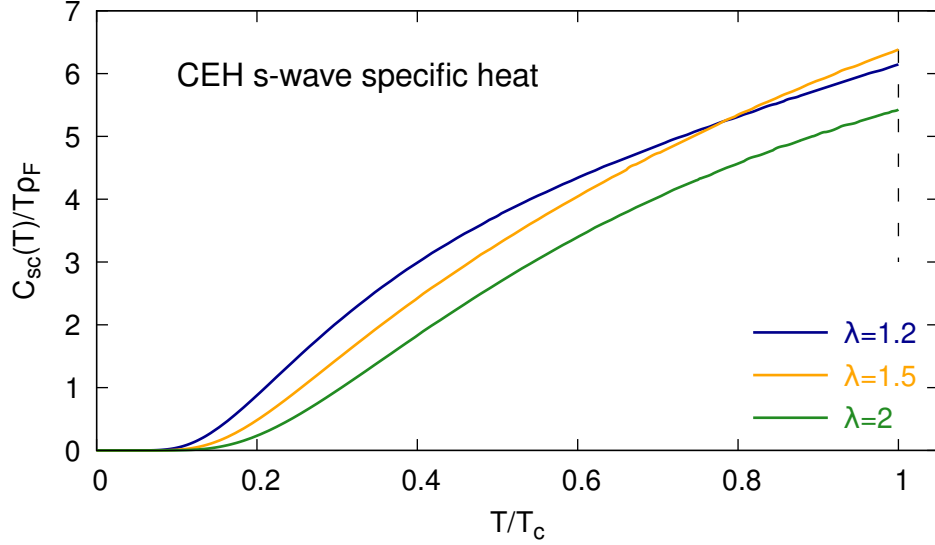


FIG. 6. The temperature dependence of heat capacity $C_{sc}(T)/(T\rho_F)$ is shown for s-wave CEH superconductivity. Cases with three different coupling parameters $\lambda = 1.2, 1.5, 2$ are presented.

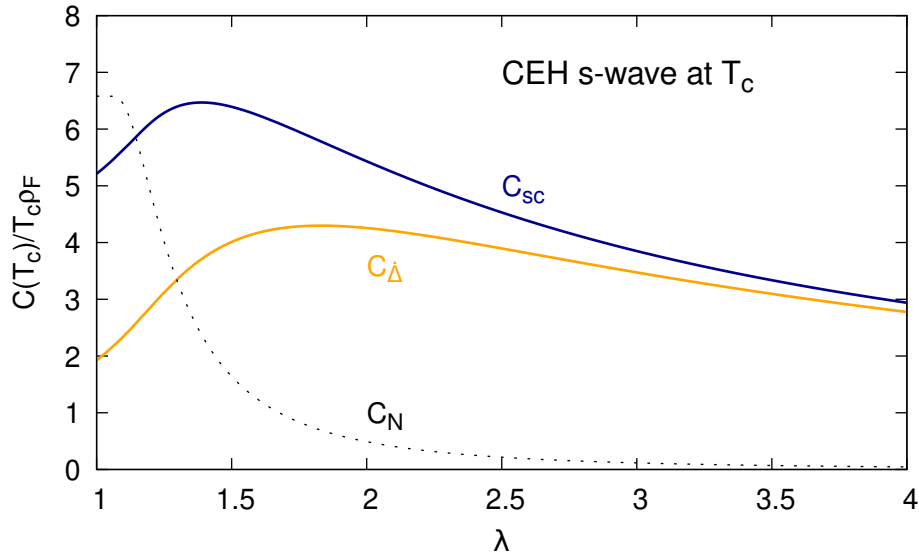


FIG. 7. The heat capacity $C_{sc}(T_c)/(T_c\rho_F)$ at $T = T_c$ as a function of λ is shown for s-wave CEH superconductivity. For comparison, the partial contribution C_{Δ} from the second term in Eq. 30 and the normal-state heat capacity C_N are also presented.

186 The CEH s-wave specific heat for various λ values is shown in Fig. 6, where it exponen-
187 tially approaches zero in the limit of $T \rightarrow 0$,

$$C_{sc}(T) \rightarrow 2T\rho_F \left(\frac{\Delta_0 - \omega^*}{T} \right)^2 e^{-(\Delta_0 - \omega^*)/T} \quad (32)$$

188 and behaves similarly to the s-wave BCS superconductivity.

189 To better understand the heat capacity jump at the critical temperature, we plot its peak
 190 value at T_c as a function of the coupling parameter λ in Fig. 7. It is evident that the second
 191 term contribution C_{Δ} in Eq. 30 dominates the heat capacity at larger λ . The normal state
 192 electronic heat capacity, within the same energy shell $\pm\omega^*$, can be written as,

$$C_N(T) = 2T\rho_F \int_{-\omega^*/T}^{\omega^*/T} dx \frac{e^x}{(e^x + 1)^2} x^2 \quad (33)$$

193 where, in the bounds of integration, $\omega^*/T = \Delta_0/(\lambda T)$ decreases rapidly as λ increases. The
 194 behavior of $C_N(T_c)$, as shown in Fig. 7, resembles that of normal metals only at very low λ
 195 values (still > 1), where ω^*/T_c remains large. It then drops rapidly to zero because ω^*/T_c
 196 approaches $2/\lambda$ asymptotically as $\lambda \rightarrow \infty$. Note that, unlike in the case of BCS, the first
 197 term in Eq. 30 does not reduce to C_N at T_c since the gap does not close at T_c or $\Delta(T_c) \neq 0$.

198 Fig. 7 demonstrates that optimal superconductivity for s-wave pairing favors relatively
 199 weaker correlations ($\lambda \lesssim 1.5$). The specific capacity jump at T_c from the superconducting
 200 state to the normal state is more complicated in CEH. The normal state electronic heat
 201 capacity in BCS maintains a constant C_N/T , giving rise to a fixed jump ratio of about 1.43
 202 for s-wave pairing. However, in CEH, this ratio varies depending on λ or the doping level
 203 and may reach about 3 at $\lambda \sim 1.5$ as C_N decreases. More complicatedly, the ω^* energy shell
 204 may shrink so significantly at larger λ or higher doping levels that other energy bands could
 205 become accessible for electrons, causing an increase in C_N and resulting in a smaller heat
 206 capacity jump at T_c .

207 B. d-wave specific heat

208 The d-wave specific heat can be similarly obtained as follows,

$$C_{sc}(T) = \frac{8T\rho_F}{\pi} \left(\int_0^{\pi/4} d\varphi d_2(\varphi, T) - \frac{\partial\Delta}{\partial T} \int_0^{\pi/4} d\varphi d_1(\varphi, T) \cos(2\varphi) \right) \quad (34)$$

209 where the two integrand functions, similar to the s-wave case, are defined by

$$d_{1,2}(\varphi, T) = \int_{(\Delta \cos(2\varphi) - \omega^*)/T}^{(\Delta \cos(2\varphi) + \omega^*)/T} dx \frac{e^x}{(e^x + 1)^2} x^{1,2} \quad (35)$$

210 and the derivative of the gap can be obtained by differentiating the gap equation,

$$\frac{\partial\Delta}{\partial T} = \frac{\Delta}{T} + \frac{\omega^*}{T} \frac{4\lambda g_2(T)}{\pi \exp(-\omega^*/T) - 8\lambda \sinh(\omega^*/T) g_1(T)} \quad (36)$$

211 where the two auxiliary functions are given by

$$g_1(T) = \int_0^{\pi/4} d\varphi \frac{e^{\Delta \cos(2\varphi)/T} \cos(2\varphi)}{(e^{(\Delta \cos(2\varphi) + \omega^*)/T} + 1)(e^{\Delta \cos(2\varphi)/T} + e^{\omega^*/T})}$$

$$g_2(T) = \int_0^{\pi/4} d\varphi \frac{1 - e^{2\Delta \cos(2\varphi)/T}}{(e^{(\Delta \cos(2\varphi) + \omega^*)/T} + 1)(e^{\Delta \cos(2\varphi)/T} + e^{\omega^*/T})}. \quad (37)$$

212 As presented in Fig. 8, the peak specific heat at $T = T_c$ for d-wave superconductivity
 213 follows the trend of s-wave, though large heat capacity jumps are extended to larger θ / λ

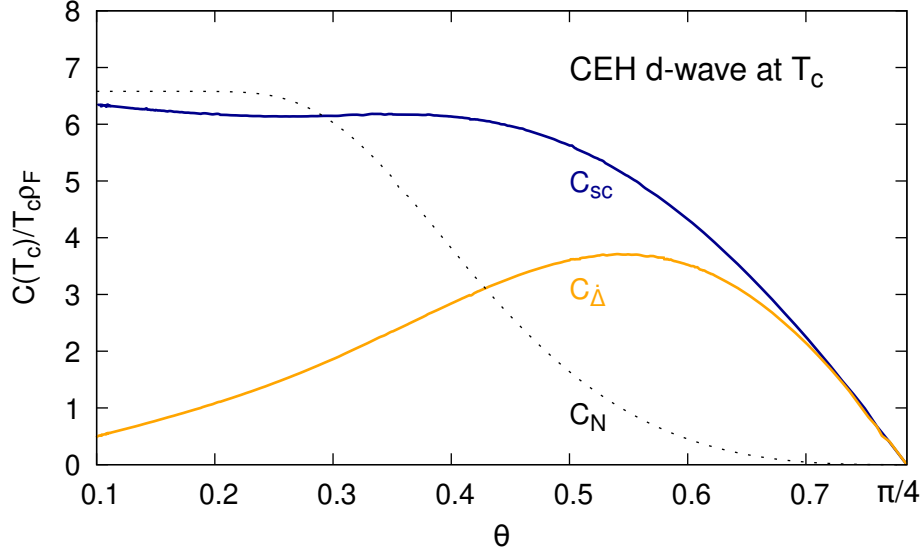


FIG. 8. The heat capacity $C_{sc}(T_c)/(T_c \rho_F)$ at $T = T_c$ as a function of θ is shown for d-wave CEH superconductivity. For comparison, the partial contribution C_{Δ} from the second term in Eq. 34 and the normal-state electronic heat capacity C_N are also presented.

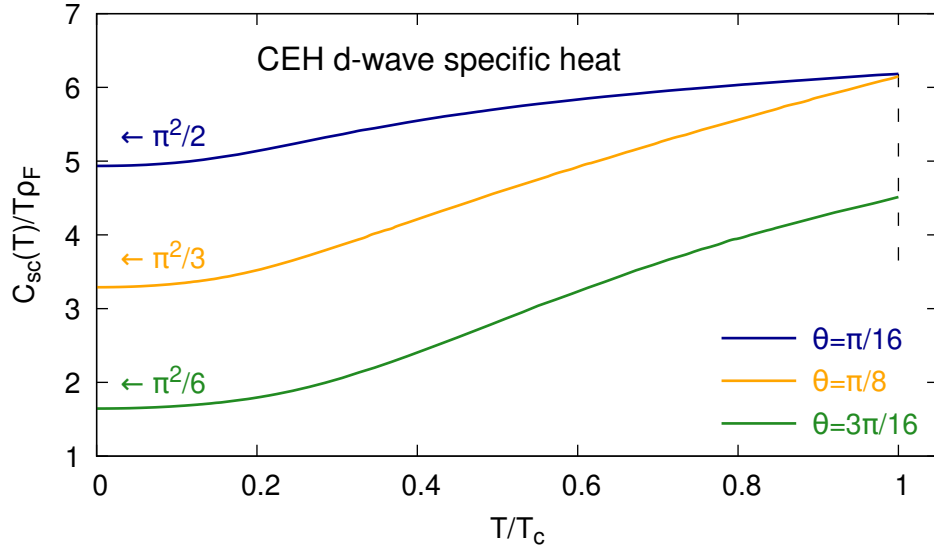


FIG. 9. The temperature dependence of heat capacity $C_{sc}(T)/(T \rho_F)$ is shown for d-wave CEH superconductivity. Cases with three different coupling strengths $\theta = \pi/16, \pi/8, 3\pi/16$ are presented.

214 or higher doping levels. Again, compared to a constant jump ratio of about 0.95 for BCS
 215 d-wave, the normalized jump ratio in CEH varies (reaching ~ 1.2 at $\lambda = 2$). The d-wave
 216 ratio is generally lower than the s-wave one due to a slower decrease in C_N as θ and λ
 217 increase.

218 One notable finding in CEH is its unique prediction of a non-zero linear term in the
 219 d-wave heat capacity at the zero-temperature limit, as shown in Fig. 9. This non-zero offset

220 originates from the $d_2(\varphi, T)$ term of Eq. 34 (see Appendix B),

$$\gamma(0) \equiv \left. \frac{C_{sc}(T)}{T} \right|_{T \rightarrow 0} = \frac{8\pi}{3} \left(\frac{\pi}{4} - \theta \right) \rho_F \neq 0 \quad (38)$$

221 which explains the “anomalous linear term” observed in the heat capacity of cuprates [22–24].
222 It only approaches zero at the extreme overdoping limit where $\theta = \pi/4$ or $\lambda \rightarrow \infty$.

223 The next leading order at $T \rightarrow 0$ in Fig. 9 is contributed from both terms (see Appendix
224 B),

$$\frac{C_{sc}(T)}{T\rho_F} - \frac{\gamma(0)}{\rho_F} \simeq \left(\frac{8\pi}{3\theta} + \frac{14\pi^3}{15 \tan 2\theta} \right) \frac{1}{\sin^2 2\theta} \left(\frac{T}{\Delta_0} \right)^2 \quad (39)$$

225 where the first part within the parentheses is calculated from the $d_1(\varphi, T)$ term and the
226 second from the $d_2(\varphi, T)$ term. This exactly explains the quadratic behavior observed in
227 the heat capacity curve of C/T at $T \ll T_c$ in d-wave superconducting cuprates [25–27].

228 V. DISCUSSIONS AND COMPARISONS WITH EXPERIMENTAL DATA

229 The proposed CEH mechanism provides many unique predictions that are distinct from
230 the well known BCS results. These differences have been discussed above in detail and are
231 also summarized in Table I. In particular, CEH naturally explains the necessity of antiferro-
232 magnetism and strong coupling in non-BCS superconductivity. Most strikingly, many of its
233 predictions agree very well with existing experimental data on non-BCS superconductors,
234 particularly cuprates and FeSCs. Several such examples will be illustrated below.

235 CEH conducts current via relative motion and this may explain why flat bands are favored
236 in high- T_c superconductivity. The key feature in CEH is the ω^* energy shell, which could
237 function as both the superconducting band for CEH pairs and an energy gap (closely related
238 to the widely-recognized pseudogap) for normal state electrons. This ω^* band may be one of
239 the flat bands where center-of-mass motion is forbidden, making it ideal for the formation
240 of antiferromagnetism and CEH pairs. For easier comparison with data below, we assume a
241 simple linear relationship between ω^* and the pseudogap temperature T^* : $\omega^* \propto T^*$.

242 In the undoped parent compound, ω^* typically exceeds the superconducting gap Δ , which
243 can disrupt the stability of CEH pairs with additional energy. Doping, however, plays a cru-
244 cial role in reducing ω^* , making it below the level of Δ , and thereby facilitating the onset
245 of superconductivity. Meanwhile, doping tends to increase the coupling parameter λ as the
246 density of states in the ω^* band rises due to unitarity or conservation of the number of quan-
247 tum states in a compressed ω^* band. High-pressure-induced superconductivity, investigated
248 in various materials, may introduce similar effects by compressing the ω^* band with external
249 pressure.

250 It have been observed in various cuprate superconductors that the ratio Δ_0/T_c exceeds
251 three. This ratio has been shown to undergo a dramatic increase with decreasing doping and
252 approach a limit of three near maximum doping (see Fig. 3 of Ref. [28] and the references
253 therein). This behavior aligns well with our d-wave prediction based on the new pairing
254 mechanism as shown in Fig. 2. To further demonstrate this, a direct comparison between
255 CEH predictions and experimental data for HgBa₂CuO_{4+ δ} (Hg-1201) [29] is presented in Fig.
256 10. A good fit to the experimental data is achieved using a simple $\lambda - p$ parametrization
257 discussed below. Furthermore, large Δ_0/T_c ratios, consistent with CEH s-wave predictions,
258 have also been observed in iron-based superconductors [12].

TABLE I. Summary of comparisons of some major results between BCS and CEH.

Model	BCS		CEH	
material	averse to magnetism		desirous of antiferromagnetism	
mechanism	Cooper pairs		chiral electron-hole pairs	
SC criteria	no constraint on Debye ω_D		$\omega^* < \Delta(T)$	
symmetry	s-wave	d-wave	s-wave	d-wave
coupling	weak coupling $\lambda \ll 1$		strong coupling $\lambda > 1$	
$E_{\mathbf{k}}^{\pm} =$	$\pm\sqrt{\xi_{\mathbf{k}}^2 + \Delta ^2}$	$\pm\sqrt{\xi_{\mathbf{k}}^2 + \Delta \cos 2\varphi ^2}$	$\xi_{\mathbf{k}} \pm \Delta $	$\xi_{\mathbf{k}} \pm \Delta \cos 2\varphi $
gap equation	$\frac{1}{\lambda} = \int_0^{\omega_D} d\xi \frac{\tanh(E^+/2T)}{E^+}$	$\frac{1}{\lambda} = \int_0^{2\pi} d\varphi \frac{\cos^2 2\varphi}{2\pi} \times \int_0^{\omega_D} d\xi \frac{\tanh(E^+/2T)}{E^+}$	Eq. 11	Eq. 12
$\Delta_0 =$	$2\omega_D e^{-1/\lambda}$	$2.426\omega_D e^{-2/\lambda}$	$\lambda\omega^*$	$\omega^*/\cos 2\theta$
T_c or $T_0 =$	$T_c = T_0$ $T_c = 1.134\omega_D e^{-1/\lambda}$	$T_c = T_0$ $T_c = 1.134\omega_D e^{-2/\lambda}$	$T_c < T_0$ $T_0 = \frac{\omega^*}{2 \tanh^{-1}(1/\lambda)}$	$T_c < T_0$ $T_0 = \frac{\omega^*}{2 \tanh^{-1}(\pi/2\lambda)}$
$\Delta_0/T_c =$	1.764	2.140	> 2 (Fig. 2)	$\gtrsim 3.077$ (Fig. 4)
$\Delta(T_c)$	$\Delta(T_c) = 0$, gap closes at T_c		$\Delta(T_c) = \omega^* \neq 0$, does not close at T_c	
$\frac{\Delta(T)}{\Delta_0}$ vs. $\frac{T}{T_c}$	dashed line in Fig. 3		Fig. 3	Fig. 5
specific heat	exponentially approaches 0		Figs. 7-6	Figs. 8-9
$C/T(T \rightarrow 0)$	exponentially approaches 0		exponentially approaches 0	quadratically approaches 0 to $\frac{8\pi}{3}(\frac{\pi}{4} - \theta)\rho_F \neq 0$
jump at T_c	1.43	0.95	varies with λ	varies with θ

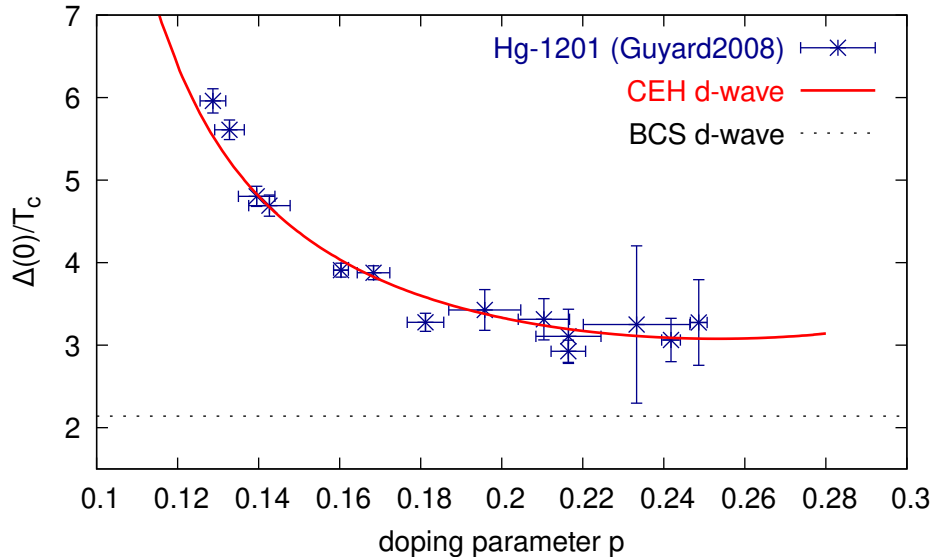


FIG. 10. Δ_0/T_c as a function of the doping level predicted by d-wave CEH is shown in good agreement with the $\text{HgBa}_2\text{CuO}_{4+\delta}$ (Hg-1201) data [29]. A much lower constant BCS value of 2.140 is also shown for comparison.

259 It has been observed in various studies (e.g., [29–31]) that the non-BCS superconducting
 260 gap does not close at the critical temperature, exhibiting a behavior similar to that shown
 261 in Fig. 5. In particular, in Fig. 3 of Ref. [29], the trend of the temperature dependence
 262 closely resembles our results and also displays a similar deviation from the BCS prediction.

263 Another piece of clear and convincing evidence comes from the detailed analysis of d-wave
 264 specific heat presented above, which is worth reiterating. CEH predicts a non-zero linear
 265 term in heat capacity at $T = 0$ for d-wave superconductors, a phenomenon well observed in
 266 many cuprates [22–24]. Furthermore, the predicted quadratic temperature dependence in
 267 C/T near zero temperature is also in agreement with observations [25–27], in stark contrast
 268 to the BCS linear dependence.

269 To make direct comparisons between CEH predictions and the wealth of data accumulated
 270 over decades of high- T_c superconductivity studies, it is necessary to establish a concrete
 271 relationship between the coupling parameter λ and the doping level parameter p . We will
 272 start with some rough yet simple estimates to facilitate direct comparisons to the data. For
 273 strongly correlated parent compounds like cuprates or FeSCs, it is reasonable to assume that
 274 the initial coupling parameter $\lambda \sim 1$. Doping then increases the density of charge carrier
 275 states, effectively making λ larger. It has been observed that the carrier density increases
 276 very rapidly at very low doping levels and then more gradually at higher doping levels [32].
 277 At low doping levels or in the case of CEH s-wave superconductors, we can approximate this
 278 with the following $\lambda - p$ relation

$$\lambda = 1 - \frac{1}{\log(p/p_m)} \quad (40)$$

279 where p_m is the maximum doping level corresponding to $\lambda \rightarrow \infty$. For the example of an
 280 s-wave FeSC discussed below, we choose to adopt $p_m = 1/3$.

281 However, CEH d-wave superconductors require larger correlations, specifically, $\lambda > \pi/2$,
 282 which means that superconductivity will not occur until the doping reaches a minimum level
 283 p_0 . To describe d-wave superconductors, we can apply the following parametrization,

$$p = p_0 + a \sin^2 \theta. \quad (41)$$

284 For the comparison shown in Fig. 10, parameters of $p_0 = 0.08$ and $a = 0.4$ are adopted.

285 Using the $\lambda - p$ and $\theta - p$ relations given in Eqs. 40-41, we can compare the phase
 286 diagrams constructed from CEH to experimental data in two examples. The first example
 287 involves $\text{NaFe}_{1-x}\text{Co}_x\text{As}$ with experimental data taken from Refs. [33, 34]. Fig. 11 shows
 288 the results from CEH assuming that $p_m = 1/3$ and $\omega^* = 0.5T^*$. The superconducting phase
 289 and T_c values derived from s-wave CEH agree well with the data. One possible issue is that
 290 T_c appears moderately overestimated at extremely low doping levels ($p \lesssim 0.01$), which could
 291 stem from the oversimplified parametrization in Eq. 40. The $\lambda - p$ relation may require more
 292 nuanced treatment at extremely low doping levels where the density of states undergoes the
 293 most significant changes. Other parameters such as the superconducting gap Δ_0 and the
 294 gap closing temperature T_0 predicted by s-wave CEH are also depicted in Fig. 11.

295 Another example is the phase diagram of $\text{La}_{2-x}\text{Sr}_x\text{CuO}_4$ (LSCO). In Fig. 12, a compar-
 296 ison between the measured LSCO data [35, 36] and the d-wave predictions from CEH ($p =$
 297 $0.05 + 0.94 \sin^2 \theta$ and $\omega^* = 1.5T^*$) is presented. The superconducting phase, characterized by
 298 the well-known dome shape for cuprates, is well reproduced and CEH shows good agreement
 299 with both the data [35] and the universal T_c parametrization of $T_c/T_c^{\text{max}} = 1 - 82.6(p - 0.16)^2$
 300 [37] using $T_c^{\text{max}} = 38K$ for LSCO.

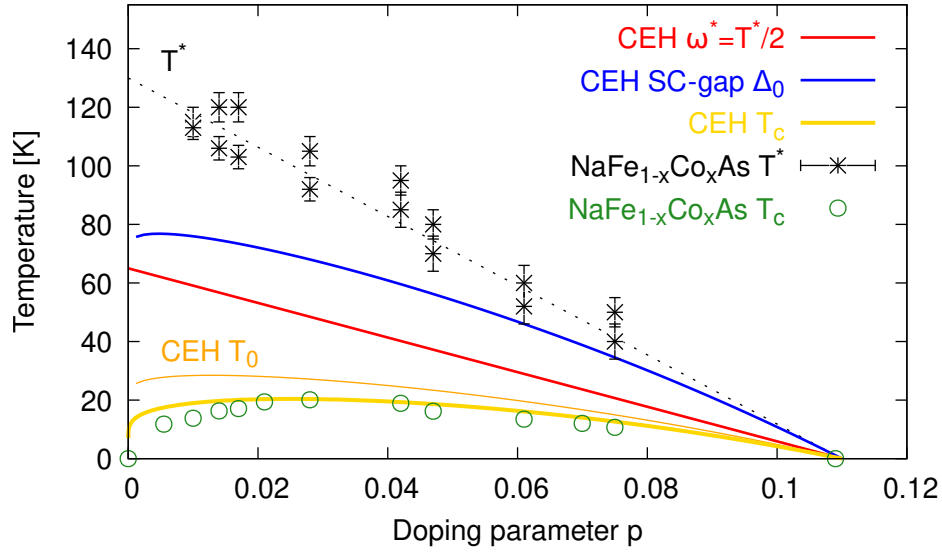


FIG. 11. Phase diagram, predicted by CEH assuming that $p_m = 1/3$ and $\omega^* = 0.5T^*$, is compared to experimental data on NaFe_{1-x}Co_xAs [33, 34].

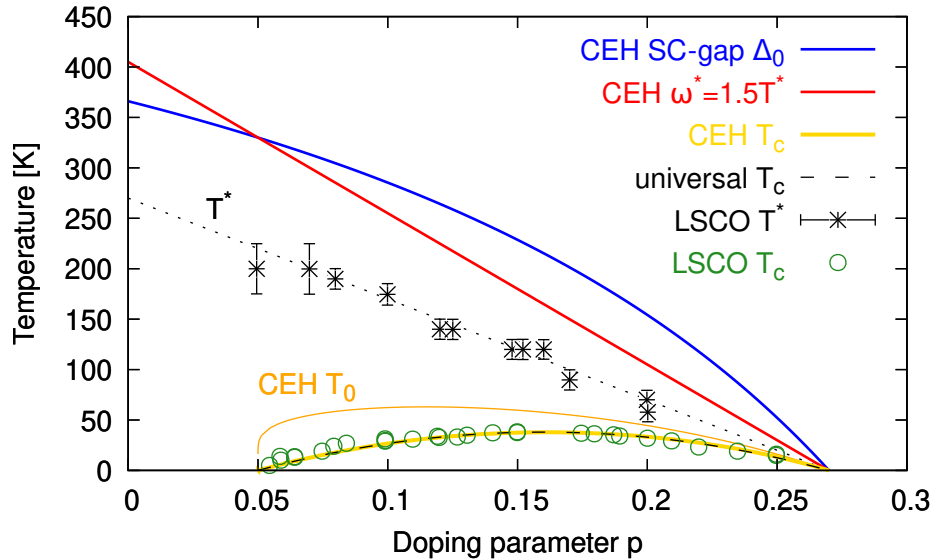


FIG. 12. Phase diagram, predicted by CEH assuming that $p = 0.05 + 0.94 \sin^2 \theta$ and $\omega^* = 1.5T^*$, is compared to experimental data on La_{2-x}Sr_xCuO₄ (LSCO) [35, 36].

301 The same $\theta - p$ relation applied in LSCO, along with $\omega^* = 2.3T^*$, also performs equally
 302 well in predicting the phase diagram of YBCO, despite significantly higher T^* and T_c val-
 303 ues in YBCO. More systematic comparisons, especially to experimental data on Δ_0 and
 304 T_0 , will provide more compelling evidence for CEH. Further comparisons with other non-
 305 BCS superconducting materials would offer more valuable insights into understanding these
 306 parametrization relations.

VI. CONCLUSIONS AND OUTLOOK

Using the new chiral electron-hole pairing mechanism, we provide a more comprehensive understanding of non-BCS superconductivity in a strongly correlated electron system. Our new predictions are remarkably consistent with numerous puzzling properties observed in cuprate and FeSC superconductors such as the unexpectedly large Δ_0/T_c ratios, the absence of gap closure at T_c , the presence of a non-zero $\gamma(0)$ term and a quadratic trend in the heat capacity ratio of C/T as $T \rightarrow 0$ in cuprates, among others. Further measurements (e.g., on T_0) and systematic comparisons with experimental data across diverse material types will provide more stringent tests on the CEH mechanism. A better understanding of the ω^* band and the λ -doping level relationship may help identify even more promising high- T_c superconducting materials in the near future.

ACKNOWLEDGMENTS

This work is supported in part by the faculty research support program at the University of Notre Dame.

Appendix A: d-wave $\lambda - \theta$ relation

The d-wave gap equation (Eq. 12) can be rewritten as,

$$\Delta(T) = \frac{4\lambda T}{\pi} \int_0^{\pi/4} d\varphi \log \left(\frac{e^{(\Delta \cos 2\varphi + \omega^*)/T} + 1}{e^{\Delta \cos 2\varphi/T} + e^{\omega^*/T}} \right). \quad (\text{A1})$$

As $T \rightarrow 0$, the integrand becomes $\Delta \cos 2\varphi/T$ if $\Delta \cos 2\varphi < \omega^*$ and ω^*/T otherwise. By introducing a new parameter θ with

$$\cos(2\theta) = \omega^*/\Delta_0 \quad (\text{A2})$$

where the range of θ is limited to $0 < \theta < \pi/4$, we obtain in the zero-temperature limit

$$\begin{aligned} \Delta_0 &= \frac{4\lambda T}{\pi} \left(\int_0^\theta d\varphi \frac{\omega^*}{T} + \int_\theta^{\pi/4} d\varphi \frac{\Delta_0 \cos 2\varphi}{T} \right) \\ &= \frac{4\theta}{\pi} \lambda \omega^* + \frac{2(1 - \sin 2\theta)}{\pi} \lambda \Delta_0 \end{aligned} \quad (\text{A3})$$

which, by using Eq. A2, immediately leads to the d-wave $\lambda - \theta$ relation as given in Eq. 22.

Appendix B: d-wave specific heat at $T \rightarrow 0$

The d-wave specific heat in Eq. 34 can be expressed as a sum of two terms: $C_{sc} = C_2 + C_1$ where $C_{2,1}$ involve the integration of the two functions $d_{2,1}(\varphi, T)$, respectively. For both terms, the integration with respect to φ can be divided into two parts: from 0 to θ' and from θ' to $\pi/4$, where $\cos 2\theta' = \omega^*/\Delta$. For convenience, we introduce the following definitions,

$$y_\pm \equiv (\cos 2\varphi \pm \cos 2\theta') \Delta/T \quad (\text{B1})$$

$$h_n(x) \equiv \frac{e^x}{(e^x + 1)^2} x^n. \quad (\text{B2})$$

332 **1. C_1 contribution at $T \rightarrow 0$**

333 First, we work with the C_1 term where we can simplify the second part of the integral as
334 follows,

$$\begin{aligned} \int_{\theta'}^{\pi/4} d\varphi \cos 2\varphi \int_{y_-}^{y_+} dx h_1(x) &= \int_{\theta'}^{\pi/4} d\varphi \cos 2\varphi \left(\int_{-y_+}^{y_+} - \int_{-y_+}^{-|y_-|} \right) dx h_1(x) \\ &= \int_{\theta'}^{\pi/4} d\varphi \cos 2\varphi \int_{|y_-|}^{y_+} dx h_1(x) \end{aligned} \quad (\text{B3})$$

335 because $h_1(x)$ is an odd function. By taking the limit of $y_+ \rightarrow \infty$ as $T \rightarrow 0$ and the following
336 integration,

$$\int_y^\infty dx h_1(x) = \log(1 + e^y) - ye^y/(e^y + 1) \equiv j(y), \quad (\text{B4})$$

337 where $j(y)$ is odd as well, we can obtain the full integration as,

$$\begin{aligned} \int_0^{\pi/4} d\varphi \cos 2\varphi \int_{y_-}^{y_+} dx h_1(x) &= \left(\int_0^{\theta'} \int_{y_-}^{y_+} + \int_{\theta'}^{\pi/4} \int_{|y_-|}^{y_+} \right) d\varphi dx \cos 2\varphi h_1(x) \\ &= \left(\int_0^{\theta'} + \int_{\theta'}^{\pi/4} \right) d\varphi \cos 2\varphi j(|y_-|). \end{aligned} \quad (\text{B5})$$

338 By a change of variable from φ to y_- , we obtain for the first part,

$$\begin{aligned} \int_0^{\theta'} d\varphi \cos 2\varphi j(y_-) &= \int_0^{(1-\cos 2\theta')\Delta/T} dy_- j(y_-) \frac{T}{2 \tan 2\varphi \Delta} \\ &= \frac{\pi^2 T}{12 \tan 2\theta' \Delta} \end{aligned} \quad (\text{B6})$$

339 where the main contribution arises from the vicinity of $\varphi \sim \theta'$, allowing us to approximate
340 $\tan 2\varphi$ with $\tan 2\theta'$, and the upper limit of integration becomes ∞ as $T \rightarrow 0$, allowing us to
341 use the identity $\int_0^\infty dy j(y) = \pi^2/6$. Likewise, the second part of the integral yields the same
342 result.

343 From Eq. 25, we can obtain the derivative of the gap,

$$\frac{\partial \Delta(T)}{\partial T} = -\frac{2T}{\theta' \sin(2\theta') \cos(2\theta') \Delta}. \quad (\text{B7})$$

344 Putting them all together, we can obtain the C_1 contribution to the specific heat,

$$\frac{C_1}{T\rho_f} = \frac{8\pi}{3\theta' \sin^2 2\theta'} \left(\frac{T}{\Delta} \right)^2 \quad (\text{B8})$$

345 which gives the first term in Eq. 39 by replacing θ' and Δ with $\theta' = \theta$ and $\Delta = \Delta_0$ at $T = 0$.

2. C_2 contribution at $T \rightarrow 0$

346

347 Similarly, contributions to the C_2 term can be separated into three parts,

$$\int_0^{\pi/4} d\varphi \int_{y_-}^{y_+} dx h_2(x) = \left(\int_0^{\theta'} \int_{y_-}^{y_+} - \int_{\theta'}^{\pi/4} \int_{|y_-|}^{y_+} + \int_{\theta'}^{\pi/4} \int_{-y_+}^{y_+} \right) d\varphi dx h_2(x) \equiv C'_{2a} + C'_{2b} + C'_{2c} \quad (\text{B9})$$

348 because $h_2(x)$ is an even function.

349 We can easily integrate out the last part by taking $y_+ \rightarrow \infty$ as $T \rightarrow 0$ and $\int_{-\infty}^{\infty} dx h_2(x) =$
350 $\pi^2/3$,

$$C'_{2c} = \int_{\theta'}^{\pi/4} d\varphi \int_{-\infty}^{\infty} dx h_2(x) = \frac{\pi^2}{3} \left(\frac{\pi}{4} - \theta' \right) \quad (\text{B10})$$

351 which gives the non-zero offset in Eq. 38.

352 The first part of Eq. B9 can be worked out by changing the order of integration as follows,

$$C'_{2a} = \left(\int_0^{x_1} \int_{\cos 2\theta'}^{Tx/\Delta + \cos 2\theta'} + \int_{x_1}^{x_2} \int_{\cos 2\theta'}^1 + \int_{x_2}^{x_3} \int_{Tx/\Delta - \cos 2\theta'}^1 \right) dx h_2(x) \frac{d \cos 2\varphi}{2 \sin 2\varphi} \quad (\text{B11})$$

353 where $x_1 = (1 - \cos 2\theta')\Delta/T$, $x_2 = 2 \cos 2\theta'\Delta/T$, or vice versa, and $x_3 = (1 + \cos 2\theta')\Delta/T$.

354 As $T \rightarrow 0$, we have $x_{1,2,3} \rightarrow \infty$, rendering the last two terms in the above integral negligible.

355 The integration with respect to φ in the first term results in $\theta' - \cos^{-1}(Tx/\Delta + \cos 2\theta')/2$.

356 Using the following expansion,

$$\cos^{-1}(t + \cos 2\theta) = 2\theta - \frac{t}{\sin 2\theta} - \frac{\cos 2\theta t^2}{2 \sin^3 2\theta} + O(t^3), \quad (\text{B12})$$

357 we can simplify the integral as

$$C'_{2a} = \frac{T}{2 \sin 2\theta' \Delta} \int_0^{\infty} dx h_3(x) + \frac{\cos 2\theta'}{4 \sin^3 2\theta} \left(\frac{T}{\Delta} \right)^2 \int_0^{\infty} dx h_4(x) + O(T^3). \quad (\text{B13})$$

358 The second part of Eq. B9 can be treated similarly as,

$$C'_{2b} = - \left(\int_0^{x_4} dx h_2(x) \int_{\cos 2\theta' - Tx/\Delta}^{\cos 2\theta'} + \int_{x_4}^{x_2} dx h_2(x) \int_{Tx/\Delta - \cos 2\theta'}^{\cos 2\theta'} \right) \frac{d \cos 2\varphi}{2 \sin 2\varphi} \quad (\text{B14})$$

359 where $x_4 = \cos 2\theta'\Delta/T$ and again, only the first term contributes. Then it can be worked

360 out as,

$$C'_{2b} = - \frac{T}{2 \sin 2\theta' \Delta} \int_0^{\infty} dx h_3(x) + \frac{\cos 2\theta'}{4 \sin^3 2\theta} \left(\frac{T}{\Delta} \right)^2 \int_0^{\infty} dx h_4(x) + O(T^3). \quad (\text{B15})$$

361 The linear terms in Eqs. B13 and B15 exactly cancel each other out. By summing up the
362 two parts and using $\int_0^{\infty} dx h_4(x) = 7\pi^4/30$, we obtain the C_2 contribution to the quadratic
363 temperature dependence, which gives the second term in Eq. 39.

364 [1] J. Bardeen, L. N. Cooper, and J. R. Schrieffer, Phys. Rev. **106**, 162 (1957).

- 365 [2] K. H. Bennemann and J. B. Ketterson, eds., *Superconductivity* (Springer, Berlin, Heidelberg,
366 2008).
- 367 [3] J. G. Bednorz and K. A. Müller, *Z. Physik B - Condensed Matter* **64**, 189 (1986).
- 368 [4] Y. Kamihara, H. Hiramatsu, M. Hirano, R. Kawamura, H. Yanagi, T. Kamiya, and H. Hosono,
369 *J. Am. Chem. Soc.* **128**, 10012 (2006).
- 370 [5] M. Ishikawa and Ø. Fischer, *Solid State Commun.* **24**, 747 (1977).
- 371 [6] R. W. McCallum, D. C. Johnston, R. N. Shelton, and M. B. Maple, *Solid State Commun.* **24**,
372 391 (1977).
- 373 [7] F. Steglich, J. Aarts, C. D. Bredl, W. Lieke, D. Meschede, W. Franz, and H. Schäfer, *Phys.*
374 *Rev. Lett.* **43**, 1892 (1979).
- 375 [8] N. D. Mathur, F. M. Grosche, S. R. Julian, I. R. Walker, D. M. Freye, R. K. W. Haselwimmer,
376 and G. G. Lonzarich, *Nature* **394**, 39 (1998).
- 377 [9] A. Lebed, R. Hull, R. M. Osgood, J. Parisi, and H. Warlimon, eds., *The Physics of Organic*
378 *Superconductors and Conductors*, Springer Series in Materials Science, Vol. 110 (Springer,
379 Berlin, Heidelberg, 2008).
- 380 [10] Y. Takabayashi and K. Prassides, *Philos. Trans. A Math. Phys. Eng. Sci.* **374**, 20150320 (2016).
- 381 [11] Z.-X. Shen, D. S. Dessau, B. O. Wells, D. M. King, W. E. Spicer, A. J. Arko, D. Marshall,
382 L. W. Lombardo, A. Kapitulnik, P. Dickinson, S. Doniach, J. DiCarlo, T. Loeser, and C. H.
383 Park, *Phys. Rev. Lett.* **70**, 1553 (1993).
- 384 [12] Y. Zhang, Z. R. Ye, Q. Q. Ge, F. Chen, J. Jiang, M. Xu, B. P. Xie, and D. L. Feng, *Nature*
385 *Phys.* **8**, 371 (2012).
- 386 [13] M. Tinkham, *Introduction to Superconductivity*, 2nd ed. (Dover Publications, Mineola, N.Y.,
387 2004).
- 388 [14] Y. Nambu and G. Jona-Lasinio, *Phys. Rev.* **122**, 345 (1961).
- 389 [15] W. Tan, *Phys. Lett. B* **797**, 134921 (2019).
- 390 [16] W. Tan, *Phys. Rev. D* **100**, 063537 (2019).
- 391 [17] W. Tan, *Int. J. Mod. Phys. D* **30**, 2142020 (2021).
- 392 [18] W. Tan, *Universe* **9**, 180 (2023).
- 393 [19] W. Tan, *Symmetry* **15**, 1415 (2023).
- 394 [20] W. Tan, Dark energy and spontaneous mirror symmetry breaking (2019).
- 395 [21] N. N. Bogoljubov, *Nuovo Cimento* **7**, 794 (1958).
- 396 [22] A. P. Ramirez, R. J. Cava, G. P. Espinosa, J. P. Remeika, B. Batlogg, S. Zahurak, and E. A.
397 Rietman, *MRS Online Proceedings Library* **99**, 459 (1987).
- 398 [23] N. E. Phillips, R. A. Fisher, J. E. Gordon, S. Kim, A. M. Stacy, M. K. Crawford, and E. M.
399 McCarron, *Phys. Rev. Lett.* **65**, 357 (1990).
- 400 [24] K. A. Kvavadze, M. M. Nadareishvili, G. G. Basiliya, D. D. Igitkhanishvili, L. A. Tarkhishvili,
401 and Sh. V. Dvali, *Phys. Solid State* **39**, 897 (1997).
- 402 [25] J. W. Loram, K. A. Mirza, J. R. Cooper, W. Y. Liang, and J. M. Wade, *J. Supercond.* **7**, 243
403 (1994).
- 404 [26] K. A. Moler, D. J. Baar, J. S. Urbach, R. Liang, W. N. Hardy, and A. Kapitulnik, *Phys. Rev.*
405 *Lett.* **73**, 2744 (1994).
- 406 [27] B. Revaz, J.-Y. Genoud, A. Junod, K. Neumaier, A. Erb, and E. Walker, *Phys. Rev. Lett.* **80**,
407 3364 (1998).
- 408 [28] D. G. Hawthorn, S. Y. Li, M. Sutherland, E. Boaknin, R. W. Hill, C. Proust, F. Ronning,
409 M. A. Tanatar, J. Paglione, L. Taillefer, D. Peets, R. Liang, D. A. Bonn, W. N. Hardy, and
410 N. N. Kolesnikov, *Phys. Rev. B* **75**, 104518 (2007).

- 411 [29] W. Guyard, M. Le Tacon, M. Cazayous, A. Sacuto, A. Georges, D. Colson, and A. Forget,
412 Phys. Rev. B **77**, 024524 (2008).
- 413 [30] M. Suzuki, T. Watanabe, and A. Matsuda, Phys. Rev. Lett. **82**, 5361 (1999).
- 414 [31] J. K. Ren, X. B. Zhu, H. F. Yu, Y. Tian, H. F. Yang, C. Z. Gu, N. L. Wang, Y. F. Ren, and
415 S. P. Zhao, Sci. Rep. **2**, 248 (2012).
- 416 [32] S. L. Cooper, G. A. Thomas, J. Orenstein, D. H. Rapkine, A. J. Millis, S.-W. Cheong, A. S.
417 Cooper, and Z. Fisk, Phys. Rev. B **41**, 11605 (1990).
- 418 [33] A. F. Wang, X. G. Luo, Y. J. Yan, J. J. Ying, Z. J. Xiang, G. J. Ye, P. Cheng, Z. Y. Li, W. J.
419 Hu, and X. H. Chen, Phys. Rev. B **85**, 224521 (2012).
- 420 [34] A. F. Wang, J. J. Ying, X. G. Luo, Y. J. Yan, D. Y. Liu, Z. J. Xiang, P. Cheng, G. J. Ye, L. J.
421 Zou, Z. Sun, and X. H. Chen, New J. Phys. **15**, 043048 (2013).
- 422 [35] K. Yamada, C. H. Lee, K. Kurahashi, J. Wada, S. Wakimoto, S. Ueki, H. Kimura, Y. Endoh,
423 S. Hosoya, G. Shirane, R. J. Birgeneau, M. Greven, M. A. Kastner, and Y. J. Kim, Phys. Rev.
424 B **57**, 6165 (1998).
- 425 [36] N. Doiron-Leyraud and L. Taillefer, Physica C Stripes and Electronic Liquid Crystals in
426 Strongly Correlated Materials, **481**, 161 (2012).
- 427 [37] M. R. Presland, J. L. Tallon, R. G. Buckley, R. S. Liu, and N. E. Flower, Physica C **176**, 95
428 (1991).